Theor Chem Acc (2011) 128:63–67
DOI 10.1007/s00214-010-0755-1

REGULAR ARTICLE

Acetonitrile adsorption and decomposition on the SnO_2 (110) surface: a first-principles computation

Xiujuan Zou · Kaining Ding · Yonfang Zhang · Shanshan Yao

Received: 11 January 2010 / Accepted: 30 March 2010 / Published online: 14 April 2010

Abstract The adsorption and decomposition of acetonitrile on the SnO_2 (110) surface were investigated by means of first-principles computations. It is found that acetonitrile could be relatively easier decomposed into CH_3 and CN fragments on the SnO_2 (110) surface than on TiO_2 (110), which agrees with the experimental results. The higher activity of the SnO_2 (110) surface than the TiO_2 (110) surface can be attributed to its higher work function and closer molecular orbital energies.

Keywords Acetonitrile · TiO_2 (110) surface · Adsorption · Decomposition

1 Introduction

As a widespread base material in conductance-type gas-sensing devices, SnO_2 has been broadly applied owing to its high sensitivity, fast response, compact size, lower power consumption and low cost [1]. Recently, SnO_2-sensing elements were used in several commercial gas sensors to detect a trace amount of the poisonous gases. Acetonitrile (ACN) is an extremely dangerous organic substance, which is poorly metabolized to cyanide ions and defined as a toxic compound in contrast to other nitriles.

ACN may dissociate on some metal oxides, such as α-Fe_2O_3 [2], ZnO [3], δ-Al_2O_3 [4], CeO_2 [5], TiO_2 [6] and also SnO_2 [1, 7]. For doped SnO_2, Lee et al. [1] proposed the possible decomposition reaction pathways of ACN gas on Pd-doped SnO_2 surface, of which the CH_3O_{ads} and CN^- adsorptions were suggested as an initial step. For clean SnO_2, Sohn et al.'s [7] experiment showed that the decomposition of ACN on SnO_2 surface was easier than those on other metal oxides like WO_3, CoO, TiO_2, etc., and the decomposition temperature of ACN on SnO_2 and TiO_2 are 130 and 230 °C, respectively. Note that both SnO_2 and TiO_2 have the same rutile-type crystallographic form. These aforementioned theoretical and experimental findings prompted us to answer the following question; does SnO_2 decompose ACN relatively easier than TiO_2? So far, no theoretical study of ACN adsorption on SnO_2 has been reported. Also the initiation mechanisms are still unclear. Thus, it is necessary to explore the reaction mechanisms of ACN adsorption and decomposition on the clean SnO_2 surface.

The SnO_2 (110) surface is the most stable surface of SnO_2. To better clarify the stable structure and the reaction mechanisms of ACN adsorption on the SnO_2 (110) surface, in this work, the structures were optimized based on reasonable models by means of density functional theory (DFT) with the generalized gradient approximation (GGA). The charge transfer, work function value and electronic structures were analyzed in detail. Furthermore, the possible reaction mechanisms were also investigated.

2 Computational method and details

All calculations were carried out with the $DMol^3$ program package in Materials Studio of Accelrys Inc [8, 9]. The generalized gradient approximation (GGA) functional by Perdew and Wang (PW91) [10] and the double numerical plus polarization (DNP) basis set were employed. The mesh size in medium quality for the numerical integration was used, and the tolerances of energy, gradient,

X. Zou · K. Ding (✉) · Y. Zhang · S. Yao
Department of Chemistry, Fuzhou University,
350002 Fuzhou, Fujian, People's Republic of China
e-mail: dknfzu@yahoo.com.cn

displacement convergence and scf convergence were 2×10^{-5} au, 4×10^{-3} au/Å, 5×10^{-3} Å and 1×10^{-5}, respectively. The real-space cutoff of atomic orbital was set at 4.5 Å, and $2 \times 3 \times 1$ k-point sampling was used. Complete linear synchronous transit and quadratic synchronous transit (LST/QST) calculations were performed to determine structures of transition state (TS), which was confirmed by additional calculations of the intrinsic reaction path. The optimized lattice parameters for bulk SnO_2 are $a = 4.782$ Å, $c = 3.325$ Å and $u = 0.306$ which are close to the experimental values ($a = 4.737$ Å, $c = 3.185$ Å, $u = 0.307$) [11] and other theoretical calculations ($a = 4.780$ Å, $c = 3.230$ Å, $u = 0.306$) [12].

Scaranto's study showed that at least a 12-atomic layers slab for CO adsorption on the rutile (110) surface should be adopted in order to achieve converging data in good agreement with the experiments [13]. Thus, in this work, a periodic slab containing fifteen atomic layers was adopted to simulate the SnO_2 (110) surface and a supercell consisting of a (3×1) surface unit cell was employed. The thickness of vacuum region between two adjacent slabs was larger than 12 Å. All the atoms including the adsorbate were fully relaxed excepted that the atoms at the bottom twelve layers were hold at their bulk positions during the geometry optimizations. The adsorption energies were calculated as the difference between the sum of the free surface ($E_{surface}$) and the gas-phase molecule ($E_{molecule}$) and the energy of the adsorption system ($E_{surface\text{-}adsorbate}$) using $E_{ads} = E_{surface} + E_{molecule} - E_{surface\text{-}adsorbate}$. With this definition, a positive E_{ads} means stable adsorption on the surface. Work function Φ is determined as an energy difference between a vacuum level E_{vac} and the Fermi energy E_F, which can be expressed as $\Phi = E_{vac} - E_F$. E_F is defined as the energy at which half of the possible energy levels in the band are occupied by electrons in terms of the Fermi–Dirac statistics, which is impossible to correctly determine for the nonmetallic systems in DFT-LDA or GGA, and E_{vac} is just the potential value at the center of the vacuum [14, 15].

3 Results and discussion

3.1 Adsorption of acetonitrile on the SnO_2 (110) surface

So far, there is not yet any direct information about the exact adsorption geometry of ACN on the SnO_2 (110) surface. Hence, in the present study, six possible adsorption sites 1–6 are explored (Fig. 1), and all the sites are considered both vertical (by N-end) and parallel arrangements of ACN molecule. Site1 is on top of a fivefold tin atom. In Site2, ACN sits on the site between two fivefold tin atoms. Site3 is on top of an in-plane oxygen atom and Site4 is on top of two in-plane oxygen atoms. Site5 is on top of a bridging oxygen atom, and in Site6 ACN interacts with two bridging oxygen atoms.

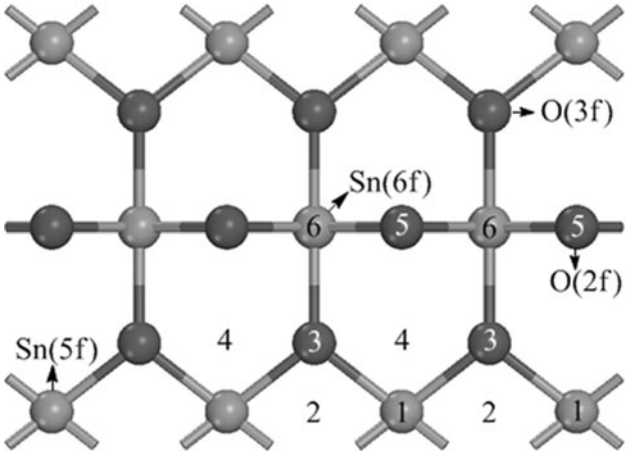

Fig. 1 *Top* view of the (3×1) SnO_2 (110) supercell: different possible adsorption sites are labeled 1–6. O (2f) and O (3f) stand for bridging oxygen and in-plane oxygen; Sn (5f) and Sn (6f) stand for fivefold tin and sixfold tin. *Black* and shining *gray* balls represent oxygen and tin atoms, respectively

After optimization, five equilibrium geometries, a–e, were obtained from different initial configurations (Fig. 2 and Table 1). Our calculated structure parameters for free ACN molecule are C_1–C_2 = 1.451 Å, $C_2 \equiv N$ =1.165 Å and θ (C_1–$C_2 \equiv N$) = 179.4°, in good agreement with experimental data [16] and other theoretically calculated values [17].

In structures a–c, ACN molecule bonds to fivefold tin atom via N atom, of which C_1–$C_2 \equiv N$ almost maintains the linear structure (θ (C_1–$C_2 \equiv N$) = 175.8°–179.4°), and C_1–C_2 bond all becomes shorter. In the other two models, d and e, ACN chains tilt away from the surface (θ (C_1–$C_2 \equiv N$) = 116.1°/125.3°), indicating that $C_2 \equiv N$ bond has lost triple-bond character. The structure of d is most favorable with 213.17 kJ/mol adsorption energy. In this case, N atom bonds to a fivefold tin (2.108 Å for N–Sn bond), and C_2 atom bonds to a bridging oxygen atom (1.436 Å for C–O bond), while the methyl group points outwards the surface with θ (C_1–$C_2 \equiv N$) angle of 116.1°. The longest C_1–C_2 and $C_2 \equiv N$ bonds are both found in structure d, from 1.451 and 1.165 Å (free ACN) to 1.592 and 1.354 Å, respectively. When C_2 atom bonds to a bridging oxygen atom, the elongation of C_1–C_2 bond and the bend of chain C_1–$C_2 \equiv N$ occur. This may be due to the coordination model change of C_2.

3.2 Electronic structures

To get a further knowledge of the electronic structure of ACN adsorption on the SnO_2 (110) surface, we performed

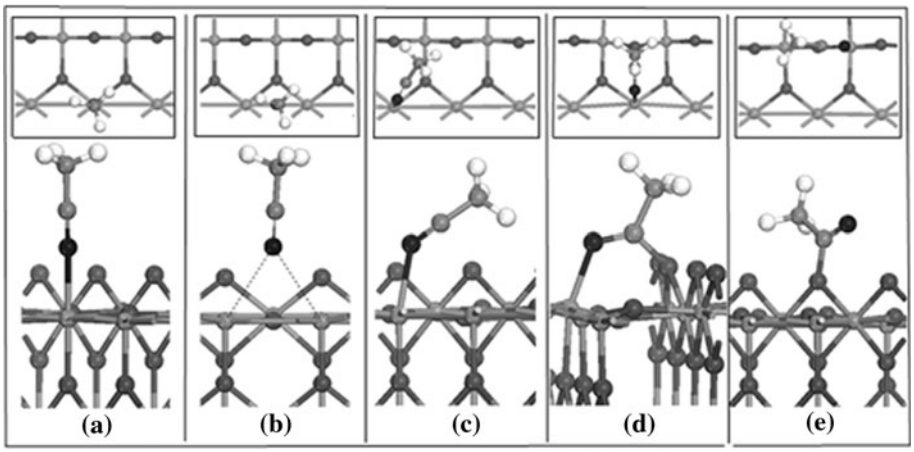

Fig. 2 The schematic *top* and *side* views of five high-symmetry starting adsorption geometries tilt to the (110) surfaces of SnO_2. *Gray*, shining *black* and *white* balls represents carbon, nitrogen and hydrogen atoms, respectively

Table 1 Structures data (distances (d) in Å and angles (θ) in °) and adsorption energy (E_{ads} in kJ/mol) for CH_3CN adsorption on the SnO_2 (110) surface

	d (C_1–C_2)	d ($C_2 \equiv N$)	θ (C_1–$C_2 \equiv$ N)	d (N–Sn_{5f})	d (C_2–O_{2f})	E_{ads}
ACN						
exp.[a]	1.460	1.157	180.0			
cal.[b]	1.467	1.170	180.0			
this work	1.451	1.165	179.4			
a	1.442	1.157	179.3	2.246	–	158.19
b	1.443	1.162	179.4	2.301/2.314	–	93.16
c	1.434	1.169	175.8	2.224	–	110.80
d	1.592	1.354	116.1	2.108	1.436	213.17
e	1.472	1.195	125.3	–	1.419	185.14

[a] Ref. [16]

[b] Ref. [17]

the Mulliken population analysis for the five stable equilibrium geometries (Table 2). Our analysis show that ACN behaves as an electron donor (Δe (ACN) = 0.199–0.529 e) and the electrons transfer from ACN to the SnO_2 (110) surface.

For the outermost valence molecular orbitals, the ground state of ACN may be represented as $(4a_1)^2$ $(5a_1)^2$ $(6a_1)^2$ $(1e)^4$ $(7a_1)^2$ $(2e)^4$ [18, 19], and its frontier orbitals are shown in Fig. 3. It can be seen that the HOMO orbital is a bonding orbital while LUMO orbital is an antibonding, and the $7a_1$ orbital is a nonbonding orbital which mainly make up of N lone pairs.

In the case of structures a and b, N atom behaves as the main electron donor (Δe (N) = 0.246 e/0.152 e), which indicates that the electrons are transferred from "N lone pairs" of ACN to substrate. Thus, the slight decreasing of $C_2 \equiv N$ bond length is both observed. Similar result is found for hydrocyanic acid adsorption on Cu (100) [20] and acetonitrile on Ni (111) [21]. Whereas, for structure d (Δe (N) = 0.201 e, Δe (C_2) = 0.306 e) and e, (Δe (N) = 0.135 e, Δe (C_2) = 0.269 e), the electrons are transferred from both N and C_2 atoms to substrate indicating that the electrons are transferred from HOMO orbital of ACN to substrate. So, the obvious elongation of $C_2 \equiv N$ bond length is observed. The same charge transfer

Table 2 Mulliken population analysis (electron charge translation from cyanide molecule to substrate, in e) for CH_3CN/SnO_2 (110) adsorption system

	C_1	C_2	N	CH_3CN	Sn (5f)	O (3f)	O (2f)
Free	−0.217	0.174	−0.261	0.000	1.430	−0.672	−0.677
a	−0.464	0.266	−0.015	0.433	1.146	−0.781	−0.762
Δe	−0.247	0.092	0.246	0.433	−0.284	−0.109	−0.085
b	−0.467	0.175	−0.109	0.199	1.266	−0.642	−0.693
Δe	−0.250	0.001	0.152	0.199	−0.164	0.030	−0.016
c	−0.467	0.542	−0.325	0.404	1.182	−0.773	−0.731
Δe	−0.250	0.368	−0.064	0.404	−0.248	−0.101	−0.054
d	−0.387	0.480	−0.060	0.529	1.127	−0.773	−0.651
Δe	−0.170	0.306	0.201	0.529	−0.303	−0.101	0.026
e	−0.387	0.443	−0.126	0.424	1.158	−0.581	−0.608
Δe	−0.170	0.269	0.135	0.424	−0.272	0.091	0.069

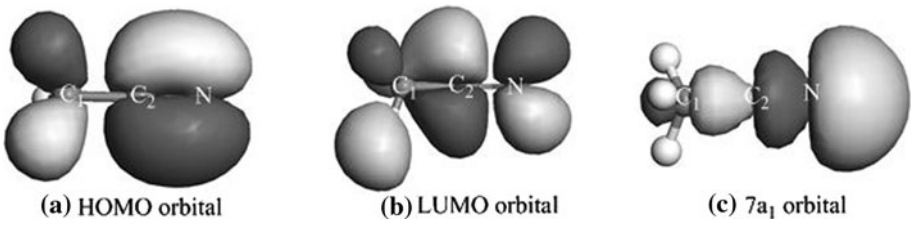

Fig. 3 The frontier orbitals of CH_3CN molecule

and bond elongation are also found for acetonitrile adsorption on Si (001) [22] and acrylonitrile on Cu (100) [23]. In structure c, N atom accepts electrons, indicating that the electrons are transferred from substrate to LUMO orbital of ACN, thus, the elongation of $C_2 \equiv N$ bond length is observed.

3.3 The reactivity of possible thermal decomposition reactions

Theoretically, in ACN, the C_1–C_2 bond is broken prior to the breakage of the $C_2 \equiv N$ bond because the binding energy of C_1–C_2 bond (518.40 kJ/mol) is lower than that of $C_2 \equiv N$ bond (770.00 kJ/mol) [24]. Previously, we demonstrated that it was relatively easier to break C_1–C_2 bond than $C_2 \equiv N$ bond on TiO_2 (110) surface [25]. Thus, in this section, the breakage of C_1–C_2 bond of CH_3CN is considered. From the aforementioned analyses, we can know that the C_1–C_2 bond of CH_3CN in structure d is weakened the most after adsorption. Thus, it is chosen as the reactant and the possible reaction step is listed as in the next paragraph.

$$CH_3CN\ (\text{chem}) \rightarrow CH_3(\text{chem}) + CN(\text{chem})$$

The energies, overall reaction pathways and structures for ACN adsorption and further thermal decomposition on the SnO_2 (110) surface are summarized in Fig. 4. The calculation shows that for this path, the energy barrier is 108.74 kJ/mol and the reaction is exothermic by 73.88 kJ/mol, indicating that ACN could dissociate on SnO_2 thermodynamically. Comparing with ACN adsorption and further thermal decomposition on the TiO_2 (110) surface (energy barrier is 136.04 kJ/mol, exothermic by 73.88 kJ/mol) [25], the energy barrier is smaller by 27.30 kJ/mol, which indicates that it is relatively easier to break the C_1–C_2 bond in ACN to form $CN_{(a)}$ species on SnO_2. This result agrees with Sohn et al.'s [7] experiments which showed that the decomposition of ACN on SnO_2 surface was easier than those on other metal oxides like TiO_2, and the decomposition temperature of ACN on SnO_2 and TiO_2 are 130 and 230 °C, respectively.

In final product, CH_3 and CN fragments are bonded to bridging oxygen and tin atoms forming OCH_3 and Sn–NC groups, respectively. For OCH_3, the calculated distance of O–C (1.427 Å) is in good agreement with experimental

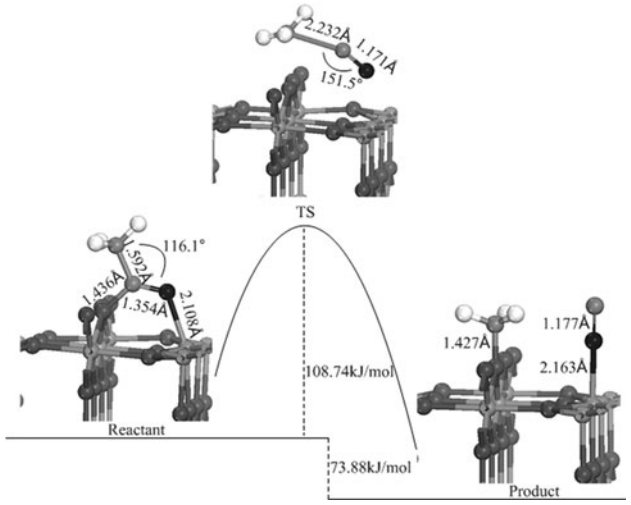

Fig. 4 The schematic reaction pathway and the corresponding structures

values of 1.420 Å [26] and for Sn–NC, the lengths of N–C and Sn–N are 1.177 and 2.163 Å, respectively. These results agree with Lee et al.'s [1] theoretical finding that the adsorbed CH_3O_{ads} and CN^- were obtained for ACN gas on Pd-doped SnO_2 surface. The similar result was also found for ACN adsorption on TiO_2 as Raskó et al.'s [6] report that ACN could decompose to form $CN_{(a)}$ species.

3.4 Work function and molecular orbital analyses

From the aforementioned analyses, we know that electrons are transferred from ACN to the SnO_2 (110) surface and the same situation occurs on TiO_2 (110) [25]. Furthermore, ACN could be relatively easier decomposed on SnO_2 than on TiO_2. To understand the difference between the SnO_2 (110) and TiO_2 (110) surface, we analyzed the work function (Φ) and molecular orbitals. It is well known that work function is a very sensitive measure of the state of the oxide surface [27]. The calculated work functions for relaxed SnO_2 (110) and TiO_2 (110) slabs are 7.12 and 6.98 eV (experiment values are 7.74 eV [28] and 7.09 eV, [27]), respectively, which indicates that SnO_2 (110) has high ability to accept electrons than TiO_2 (110). This is one of the reasons why SnO_2 and TiO_2 have different reactivities. After adsorption, the work functions for SnO_2 (110) and TiO_2 (110) slabs are 6.47 and 6.71 eV, thus $\Delta\Phi$ (work

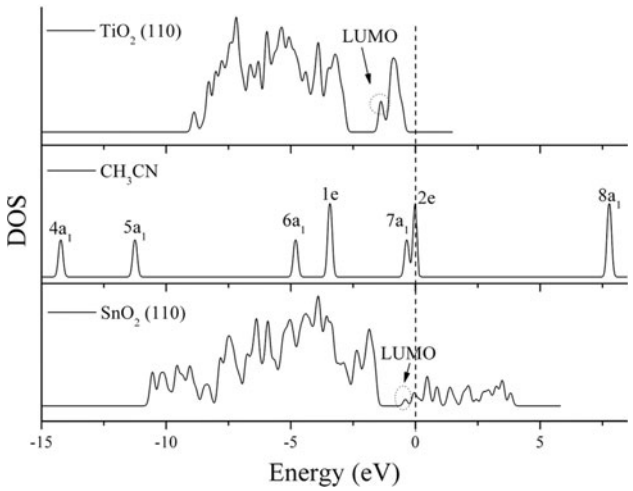

Fig. 5 Calculated DOS of TiO_2 (110), CH_3CN and SnO_2 (110). The zero energy line represents Fermi level for CH_3CN

function differences between before and after adsorption) are 0.65 and 0.27 eV, respectively. The bigger $\Delta\Phi$ further indicates that the adsorption of ACN on SnO_2 (110) is more drastic than that of on TiO_2 (110). We also analyzed the DOS of TiO_2 (110), ACN and SnO_2 (110) (Fig. 5). The LUMO of SnO_2 (110) is closer to the HOMO of ACN than that of TiO_2 (110). This orbital overlap phenomenon could be another reason for different reactivities of SnO_2 and TiO_2. From the aforementioned analysis, we can conclude that work function, $\Delta\Phi$ and orbital overlapping may account for the higher reactivity of SnO_2.

4 Conclusion

The adsorption and decomposition of acetonitrile on the clean SnO_2 (110) surface were investigated with first-principles computations. The DFT calculations reveal that in all the stable structures, the electrons are transferred from ACN to substrate, which is similar with ACN adsorption on TiO_2 (110). The reaction mechanism for the dissociation of ACN on the SnO_2 (110) surface shows that ACN could be relatively easier decomposed into NC and CH_3 fragments with energy barrier smaller by 27.30 kJ/mol than on TiO_2 (110). This result agrees with Sohn et al.'s report that the decomposition of ACN on SnO_2 surface was easier than that of other metal oxides like TiO_2, and the decomposition temperature of ACN on SnO_2 and TiO_2 are 130 and 230 °C, respectively. We also analyzed the work function and molecular orbitals and concluded that the higher work function and closer energy orbitals can account for the higher activity of SnO_2 surface.

Acknowledgments This work was supported by the NSF of China (Grant 20773024), Education Foundation of Fujian province (No. JA09015) and the programs for New Century Excellent Talents in University of Fujian Province (HX2006-97).

References

1. Lee MJ, Cheong HW, Son LDN, Yoon YS (2008) Jpn J Appl Phys 47:2119
2. Lorenzelli V, Busca G, Sheppard N (1980) J Catal 66:28
3. Lavalley JC, Gain C (1979) C R Acad Sci Paris Ser C 288:177
4. Krietenbrink H, Knozinger H (1976) Z Phys Chem (Wiesbaden) 102:43
5. Binet C, Jadi A, Lavalley JC (1992) J Chem Phys 89:31
6. Raskó J, Kiss J (2006) Catal Lett 109:71
7. Sohn JR, Park HD, Lee DD (2000) Appl Surf Sci 161:78
8. Payne MC, Allan DC, Arias TA, Joannopoulos JD (1992) Rev Mod Phys 64:1045
9. Milman V, Winkler B, White JA, Pickard CJ, Payne MC, Akhmataskaya EV, Nobes RH (2000) Int J Quantum Chem 77:895
10. Perdew JP, Wang Y (1992) Phys Rev B 45:13244
11. Wyckoff R (1964) Crystal Structures. Wiley, New York
12. Oviedo J, Gillan MJ (2000) Surf Sci 467:35
13. Scaranto J, Giorgianni S (2009) Chem Phys Lett 473:179
14. Liu W, Zheng WT, Jiang Q (2007) Phys Rev B 75:235322
15. Askeland DR, Phulé PP (2004) The science and engineering of materials. Thomson Brooks/Cols, Pacific Grove
16. Vijay A, Sathyanarayana DN (1996) J Phys Chem 100:75
17. Seo JS, Cheong BS, Cho HG (2002) Spectrochim Acta A 58:1747
18. Eden S, Limão-Vieira P, Kendall P, Mason NJ, Hoffmann SV, Spyrou SM (2003) Eur Phys J D 26:201
19. Delwiche J, Gochel-Dupuis M, Collin JE, Heinesch J (1993) J Electron Spectrosc Rel Phenom 66:65
20. Hu JM, Li Y, Li JQ, Zhang YF, Zhou LX (2003) Acta Chim Sin 61:476
21. Bigot B, Delbecq F, Peuch VH (1995) Langmuir 11:3829
22. Rangan S, Bourmel F, Gallet JJ, Kubsky S, Guen KL, Dufour G, Rochet F, Sirotti F (2005) Phys Rev B 71:165319
23. Xia SW, Gao N, Xu X, Sun YL, Xia SW (2006) Acta Chim Sin 64:27
24. David RL (2003–2004) CRC handbook of chemistry and physics, 84th edn. CRC Press, Baco Raton
25. Zou XJ, Ding KN, Zhang YF, Li JQ (2010) Int J Quantum Chem. doi:10.1002/qua.22454
26. Hofmann P, Schindler KM, Bao S, Fritzsche V, Ricken DE, Bradshaw AM, Woodruff DP (1994) Surf Sci 304:74
27. Kiejna A, Pabisiak T, Gao SW (2006) J Phys Condens Matter 18:4207
28. Godin TJ, Lafemina JP (1993) Phys Rev B 47:6518